

# Photoproduction of the scalar mesons $f_0(500)$ and $f_0(980)$ off the nucleon

Je-Hee Lee,<sup>1,2,\*</sup> Hyun-Chul Kim,<sup>1,3,†</sup> Sang-Ho Kim,<sup>4,‡</sup> Hui-Young Ryu,<sup>5,§</sup> and Byung-Geel Yu<sup>6,¶</sup>

<sup>1</sup>*Department of Physics, Inha University, Incheon 22212, Republic of Korea*

<sup>2</sup>*RIKEN Nishina Center, RIKEN, 2-1 Hirosawa, 351-0115 Saitama, Japan*

<sup>3</sup>*School of Physics, Korea Institute for Advanced Study (KIAS), Seoul 02455, Republic of Korea*

<sup>4</sup>*Asia Pacific Center for Theoretical Physics (APCTP), Pohang 37673, Republic of Korea*

<sup>5</sup>*Department of Physics, Pusan National University, Busan 46241, Republic of Korea*

<sup>6</sup>*Research Institute for Basic Sciences, Korea Aerospace University, Goyang 10540, Republic of Korea*

(Dated: October 27, 2021)

We investigate photoproduction of the scalar mesons off the nucleon, using the effective Lagrangians and the Regge approach. We first study  $f_0(980)$  photoproduction, replacing the Feynman propagator with the Regge ones for  $\rho$ -meson exchange in the  $t$ -channel. The model parameters are fixed by reproducing the experimental data on the differential cross section. We then apply the same method to  $f_0(500)$  or  $\sigma$  photoproduction with the same parameters for the Regge propagator. Since the threshold energy of the  $f_0(500)$  production is rather low,  $N^*$  resonances, which can decay into the nucleon and two pions in the isoscalar and scalar state, can come into play in the  $s$ -channel. To examine the effects of the  $N^*$  resonances, we set up two models to look into the respective contribution of the  $N^*$  resonances. We find that in particular  $N(1440)$  and  $N(1680)$  play important roles in  $f_0(500)$  photoproduction. We discuss the physical implications of the present results.

PACS numbers: 13.60.-r, 13.60.Le, 14.20.Gk, 14.40.Be

Keywords:  $f_0$  photoproduction,  $N^*$  resonances

arXiv:1608.01508v3 [hep-ph] 19 Jul 2017

---

\* jehee.lee@inha.edu

† hchkim@inha.ac.kr

‡ sangho.kim@apctp.org

§ hyryu2015@knu.ac.kr

¶ bgyu@kau.ac.kr

## I. INTRODUCTION

Understanding the structure of low-lying scalar mesons has been one of the most challenging issues in hadronic physics. Their internal structure is still under debate. That the  $f_0(500)$  scalar meson, which is also known as  $\sigma$ , is not an ordinary meson consisting of a quark and an anti-quark is more or less in consensus. Recent studies suggest that these scalar mesons may belong to the flavor SU(3) non- $q\bar{q}$  nonet (see reviews [1, 2], a “note on scalar mesons below 2 GeV” in Ref. [3], and references therein. A recent review provides also various information on the structure of the scalar meson [4], including a historical background of the  $\sigma$  meson). The  $f_0(500)$  is also interpreted as one of the glueballs or gluonia, mixed with the  $\bar{q}q$  state [5–7], though this idea is criticized because the same analysis is rather difficult to be applied to explaining the strange scalar meson  $K_0^*(800)$  or  $\kappa$ , which is also considered as a member of the nonet. The  $f_0(500)$  is often regarded as a tetraquark state in a broad sense [8]. The  $f_0(500)$  as a tetraquark state has a multiple meaning: It can be described as a diquark-antidiquark correlated state [9, 10],  $\bar{q}q\bar{q}q$  state [11], or correlated  $2\pi$  state [12, 13] arising from  $\pi\pi$  scattering. This non  $\bar{q}q$  feature was employed in various theoretical approaches such as QCD sum rules [14], effective Lagrangians [15], and lattice QCD [16–18].

The scalar mesons were also extensively studied phenomenologically. There are two scalar-isoscalar mesons ( $I^G(J^{PC}) = 0^+(0^{++})$ ) below 1 GeV, that is, the lowest-lying  $f_0(500)$  (or  $\sigma$ ) and the first excited  $f_0(980)$ . Both the  $f_0(500)$  and the  $f_0(980)$  exist in  $\pi\pi$  scattering and their pole positions were investigated based on many different processes, for example, such as  $\pi N \rightarrow \pi\pi N$  reactions [19–21],  $K_{l4}$  decay [22, 23],  $D \rightarrow 3\pi$  [24, 25],  $J/\psi \rightarrow \omega\pi\pi$  [26],  $\psi(2S) \rightarrow \pi^+\pi^- J/\psi$  [27],  $\gamma\gamma \rightarrow \pi\pi$  [28],  $pp$  scattering [29], and so on (for details, we refer to Refs. [3, 4]). While the mass and the width of the  $f_0(980)$  are more or less known to be  $m_{f_0} = 990 \pm 20$  MeV and  $\Gamma = 40 - 100$  MeV, those of  $f_0(500)$  are still far from consensus (see Ref. [3]). The upper bound of the  $f_0(500)$  mass is given in the large  $N_c$  limit in terms of the Gasser-Leutwyler low-energy constant [30], which suggests that the  $f_0$  mass is quite possibly smaller than 700 MeV.

While there was a great deal of theoretical works on the structure of the  $f_0(500)$ , its reaction mechanism was less investigated. Recently, the CLAS Collaboration has reported the first analysis of the  $S$ -wave photoproduction of  $\pi^+\pi^-$  pairs in the region of the  $f_0(980)$  at photon energies between 3.0 and 3.8 GeV and momentum transfer squared  $-t$  between  $0.4 \text{ GeV}^2$  and  $1 \text{ GeV}^2$  [31, 32]. While the differential cross section for the  $\gamma p \rightarrow \pi^+\pi^- p$  process in the  $S$ -wave shows an evident signal for the  $f_0(980)$  production, the  $f_0(500)$  was not seen clearly. However, there is still a hint for the existence of the  $f_0(500)$  in  $\pi^+\pi^- p$  photoproduction measured at different kinematic conditions [33]. Thus, it is of great interest to study the  $\gamma p \rightarrow \pi^+\pi^- p$  reaction in the scalar and isoscalar channel. Since these two pions are strongly correlated, one has to consider the rescattering effects of these two pions to describe  $\gamma p \rightarrow \pi^+\pi^- p$  in the scalar and isoscalar channel, which are essential in order to explain the production mechanism of the scalar and isoscalar mesons  $f_0$  quantitatively in  $\pi^+\pi^- p$  photoproduction. Moreover, it is crucial to take into account the  $K\bar{K}$  channel in addition [34], since its threshold is open in the vicinity of the  $f_0(980)$  mass. In order to take into account the effects of the  $K\bar{K}$  channel, one has to introduce the coupled-channel formalism, which requires the fully coupled  $\pi\pi$  and  $K\bar{K}$  amplitudes.

However, before we carry out the investigation on the  $\gamma p \rightarrow \pi^+\pi^- p$  reaction, we need to examine the related two-body process  $\gamma p \rightarrow f_0 p$  as a first step toward more complicated correlated  $\pi\pi$  photoproduction. Moreover, since the CLAS Collaboration already presented the differential cross section for  $f_0(980)$  photoproduction in the photon energy range  $E_\gamma = (3.0 - 3.8)$  GeV, it is important to study  $f_0$  photoproduction theoretically as well before we examine the  $\gamma p \rightarrow \pi^+\pi^- p$  process with pion pairs in the  $S$ -wave. In addition to  $f_0(980)$  photoproduction, we study in the present work the  $f_0(500)$  production by photon beams, based on effective Lagrangians and a Regge approach. The Regge exchange in  $f_0(980)$  photoproduction was already applied in Ref. [35] with the same Regge trajectory but a different set of parameters. We will first compute the differential cross section for  $f_0(980)$  photoproduction and compare the results with the CLAS experimental data such that we can fix parameters for the  $t$ -channel Reggeon exchange. Since there is no excited nucleon that decays into  $\pi^+\pi^-$  pairs in the  $S$ -wave beyond the  $f_0(980)N$  threshold, we consider only the  $N$  exchange in the  $s$  channel. Then we will proceed to study  $f_0(500)$  photoproduction with the same parameters for the Reggeon, which is fixed in  $f_0(980)$  production. As far as  $f_0(500)$  photoproduction is concerned, we need to consider several excited nucleons above the threshold energy, which can decay into  $\pi^+\pi^- N$ , where the pion pairs are in the isoscalar and scalar wave.

Upon computing the transition amplitude for the  $f_0(500)$  photoproduction, there are ambiguities to which we have to pay attention carefully. Firstly, the width of the  $f_0(500)$  is very large, so that the value of the  $f_0(500)$  mass is quite uncertain. Thus, we have to look into the dependence of the results on the  $f_0(500)$  mass. Secondly, the photocoupling constant  $g_{\gamma\sigma\rho}$  is experimentally not much known. Though there are several theoretical suggestions on its value, the agreement has not been reached yet. Experimentally, two relevant decay channels are known:  $\rho^0 \rightarrow \pi^+\pi^-\gamma$  [36, 37] and  $\rho^0 \rightarrow \pi^0\pi^0\gamma$  [38, 39]. To see the contribution of the  $f_0(500)$  in these decay processes, one has to reply on models. So, it is required to examine uncertainties arising from the coupling constant  $g_{\gamma\sigma\rho}$ . In principle,  $\omega$ -meson exchange could be considered. However, the branching ratio of  $\omega \rightarrow \pi^+\pi^-\gamma$  is not much known: its experimental

upper bound is given as  $< 3.6 \times 10^{-3}$  with CL=95%. On the other hand,  $\rho \rightarrow \pi^+\pi^-\gamma$  is experimentally known to be  $(9.9 \pm 1.6) \times 10^{-3}$  [3]. Thus, the value of the  $\gamma f_0 \rho$  coupling constant is expected to be much larger than that of  $\omega \rightarrow f_0 \gamma$ , based on the experimental data given above. We have confirmed numerically that the effect of  $\omega$ -exchange is indeed much smaller than that of  $\rho$ -exchange. So, we will ignore in this work the contribution from  $\omega$ -meson exchange. Thirdly, the final state in the  $N^* \rightarrow (\pi\pi)_{S\text{-wave}}^{I=0} N$  decay should contain both the background  $\pi\pi$  and the  $f_0(500)$  resonance. It indicates that it is rather difficult to determine the coupling constants for the  $f_0(500)NN^*$  unambiguously. Considering these points that will bring about the uncertainties of the present work, we have to introduce certain assumptions before we proceed to investigate  $f_0(500)$  photoproduction. Though we will take 500 MeV as a main value for the  $f_0(500)$  mass in this work, we will carefully examine the dependence of the results for the total cross section on the mass of the lowest-lying scalar meson. Lastly, we will regard  $\pi^+\pi^-$  pairs in the  $S$ -wave as the  $f_0(500)$  meson, which are produced in the course of the  $N^* \rightarrow (\pi^+\pi^-)_{S\text{-wave}}^{I=0} N$  decays, so that we are able to determine the strong coupling constants for the  $N^* \rightarrow f_0(500)N$  transitions. Since the  $f_0(500)$  resonance is the most dominant one in  $\pi\pi$  scattering in the scalar-isoscalar channel, this approximation is rather plausible.

In addition to the Roper resonance, we want to consider other  $N^*$  resonances that can decay into  $(\pi\pi)_{S\text{-wave}}^{I=0} N$ . Referring to Ref. [3], we find that 10 excited nucleon resonances have the decay channel of  $N^* \rightarrow (\pi\pi)_{S\text{-wave}}^{I=0} N$ . However, there are not enough data for  $N^* \rightarrow (\pi\pi)_{S\text{-wave}}^{I=0}$  except for  $N(1440)$ ,  $N(1680)$ , and  $N(1880)$ . Since  $N(1880)$  has an overall status 2 star, we will not consider it (see the review “ $N$  and  $\Delta$  resonances” in Ref. [3]). Thus, we expect that the main contribution will come from  $N(1440)$  and  $N(1680)$ . As will see later,  $N(1680)$  provides predominantly a large contribution to the total cross section. Thus, we will set up two different models to delve into each contribution from the  $N^*$  resonances. In Model I, we will include those with spin 1/2 and an overall status 3 or 4 stars. Thus, we consider  $N(1535)1/2^-$ ,  $N(1650)1/2^-$ , and  $N(1710)1/2^+$  in addition to  $N(1440)1/2^+$ , though their data are not much known. In Model II, we further take into account  $N(1520)3/2^-$ ,  $N(1675)5/2^-$  and  $N(1680)5/2^+$  together with those included in Model I.

The present work is sketched as follows: In Section II, we explain the general formalism for the  $f_0(980)$  and  $f_0(500)$  photoproductions. In Section III, we present the numerical results separately for Model I and Model II, and discuss their physical implications. The last Section is devoted to the summary and the conclusion of the present work. We also discuss perspectives of future works in the last Section.

## II. GENERAL FORMALISM

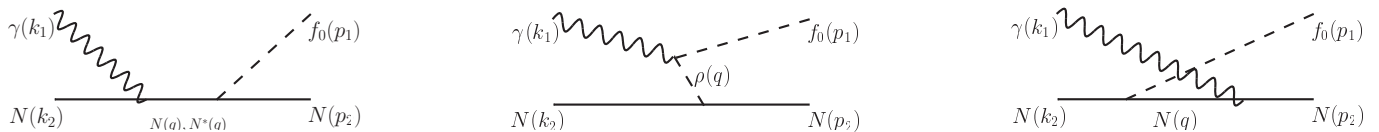


FIG. 1. Feynman diagrams for  $f_0$  photoproduction at the tree level. Each diagram corresponds to the  $s$  channel, the  $t$  channel, and the  $u$  channel in order.

We start with the tree-level Feynman diagrams relevant to the  $\gamma p \rightarrow f_0(980)p$  and  $\gamma p \rightarrow f_0(500)p$  reactions based on the effective Lagrangian approach, as depicted in Fig. 1. Note that we will not consider any contribution from  $N^*$  resonances to  $f_0(980)$  photoproduction, since the threshold energy of its production is rather high. There is no  $N^*$  above 1900 MeV, which can decay into  $f_0(980)N$ . Thus, we take only into account nucleon exchange both in the  $s$ - and  $u$ - channels. As far as the  $t$ -channel diagram is concerned,  $\rho$ -meson exchange comes into play. However, the  $\gamma N \rightarrow f_0(980)N$  reaction was experimentally measured at higher photon energies ( $E_\gamma = 3.0 - 3.8$  GeV) [31, 32], which is quite far beyond threshold. Since the method of effective Lagrangians is devised for describing the mechanism of hadronic reactions near threshold, we need to revise it to explain  $f_0(980)$  photoproduction at higher  $E_\gamma$ . We will employ a hybridized Regge approach in which the Feynman propagator in the  $t$  channel is replaced with the Regge propagator for  $\rho$ -meson exchange, while the coupling constants and spin structures are taken from the effective Lagrangians. This approach was successfully used for describing the productions of strange and charmed hadrons [40–42]. A virtue of using this hybridized Regge model is that we can use the reggeized  $\rho$  meson in the  $t$  channel also for  $f_0(500)$  photoproduction with the same parameters fixed in  $f_0(980)$  photoproduction.

As for the  $\gamma N \rightarrow f_0(500)N$  reaction, we include the  $\rho$  Reggeon in the  $t$  channel with the same parameters used in  $f_0(980)$  photoproduction. In the  $s$ - and  $u$ -channels, we consider nucleon exchange. Since the threshold energy of  $f_0(500)$  photoproduction is about 1.4 – 1.5 GeV, we need to introduce in the  $s$  channel the  $N^*$  resonances that decay only into  $(\pi\pi)_{S\text{-wave}}^{I=0} N$ . To study the contributions of the  $N^*$  resonances, we develop two different models: In Model I, we include  $N(1440)1/2^+$ ,  $N(1535)1/2^-$ ,  $N(1650)1/2^-$ , and  $N(1710)1/2^+$ , while Model II further contains

$N(1520)3/2^-$ ,  $N(1675)5/2^-$  and  $N(1680)5/2^+$  with higher spins in addition to those in Model I. Kinematics of the  $\gamma p \rightarrow f_0 p$  reactions are given as shown in Fig. 1:  $k_1$  and  $k_2$  stand for the four momenta respectively for the photon and the nucleon in the initial state, whereas  $p_1$  and  $p_2$  designate those respectively for the  $f_0$  and the nucleon in the final state.

### A. Model I

As we have already briefly mentioned in Introduction, there are ten excited nucleon resonances that can decay into  $f_0(500)N$ . However, if we consider  $N^*$  with overall status 3 or 4 star, then there are only seven  $N^*$  resonances. In order to scrutinize the effects of the  $N^*$  resonances carefully, we first introduce the pertinent  $N^*$  resonances only with spin 1/2 to describe  $f_0(500)$  photoproduction. We call this *Model I*.

To compute the Feynman invariant amplitudes for  $f_0$  photoproduction, we use the following effective Lagrangians [43–46]:

$$\begin{aligned}
\mathcal{L}_{\gamma f_0 \rho} &= \frac{eg_{\gamma f_0 \rho}}{2m_\rho} \partial_\mu A_\nu (\partial^\mu \rho^\nu - \partial^\nu \rho^\mu) f_0, \\
\mathcal{L}_{\gamma NN} &= -\bar{N} \left( e_N \gamma_\mu A^\mu - \frac{e\kappa_N}{2m_N} \sigma_{\mu\nu} \partial^\nu A^\mu \right) N, \\
\mathcal{L}_{\rho NN} &= -g_{\rho NN} \bar{N} \left( \gamma_\mu \rho^\mu - \frac{\kappa_\rho}{2m_N} \sigma_{\mu\nu} \partial^\nu \rho^\mu \right) N, \\
\mathcal{L}_{f_0 NN} &= g_{f_0 NN} f_0 \bar{N} N, \\
\mathcal{L}_{\gamma NN^*(\frac{1}{2}^\pm)} &= \frac{ef_1}{2m_N} \bar{N} \Gamma^{(\mp)} \sigma_{\mu\nu} \partial^\nu A^\mu N^* + \text{H.c.}, \\
\mathcal{L}_{f_0 NN^*(\frac{1}{2}^\pm)} &= \pm g_{f_0 NN^*} f_0 \bar{N} \Gamma^{(\mp)} N^* + \text{H.c.},
\end{aligned} \tag{1}$$

where  $A$ ,  $N$ ,  $\rho$ , and  $f_0$  denote the photon, the nucleon, the  $\rho(770, 1^-)$ , and the  $f_0$  fields, respectively. The  $N^*$  represents a field for the excited nucleon. The values of the coupling constants given in the Lagrangians will be discussed later. The matrix  $\Gamma^{(\pm)}$  depends on the parity of the  $N^*$  resonance and is defined as

$$\Gamma^{(+)} = \gamma_5, \quad \Gamma^{(-)} = \mathbf{1}. \tag{2}$$

Based on the effective Lagrangians in Eq. (1), we can compute the Feynman invariant amplitudes for each channel as follows:

$$\begin{aligned}
-i\mathcal{M}_{t(\rho)} &= \frac{ieg_{\gamma f_0 \rho} g_{\rho NN}}{2m_\rho} \bar{u}(p_2) \frac{1}{t - m_\rho^2} \left[ \epsilon^\alpha (k_1 \cdot p_1) - k_1^\alpha (\epsilon \cdot p_1) \right] \left[ \gamma_\alpha - \frac{ik_\rho}{2m_N} \sigma_{\alpha\beta} q_t^\beta \right] u(k_2), \\
-i\mathcal{M}_{s(N)} &= ig_{f_0 NN} \bar{u}(p_2) \frac{q_s + m_N}{s - m_N^2} \not{\epsilon} \left[ e_N - \frac{e\kappa_N}{2m_N} \not{k}_1 \right] u(k_2), \\
-i\mathcal{M}_{u(N)} &= ig_{f_0 NN} \bar{u}(p_2) \not{\epsilon} \left[ e_N - \frac{e\kappa_N}{2m_N} \not{k}_1 \right] \frac{q_u + m_N}{u - m_N^2} u(k_2),
\end{aligned} \tag{3}$$

where the momentum transfers are given as  $q_t = p_1 - k_1$ ,  $q_s = k_1 + k_2$ , and  $q_u = p_2 - k_1$ .  $e_N$  is the electric charge of the nucleon and  $\epsilon_\mu$  indicates the polarization vector of the photon. The  $u(p_2)$  and  $u(k_2)$  denote the Dirac spinors of the outgoing nucleon and the incoming nucleon, respectively. The  $m_N$  and  $m_\rho$  stand for the masses of the nucleon and  $\rho$  meson, respectively.  $t$ ,  $s$ , and  $u$  represent the Mandelstam variables and are defined as

$$t = (p_1 - k_1)^2, \quad s = (k_1 + k_2)^2, \quad u = (p_2 - k_1)^2. \tag{4}$$

The effective Lagrangian approach has been successfully used to describe hadronic reaction in the low-energy region. However, when the photon energy increases, the results from the effective Lagrangians start to deviate from the data and do not even satisfy the unitarity [41]. Since the CLAS data on  $f_0(980)$  photoproduction was conducted at  $E_\gamma = 3.0$  GeV and  $E_\gamma = 3.8$  GeV, which is far from threshold, the effective Lagrangian method is not suitable to explain the data. Thus, we employ a hybridized Regge model as already mentioned previously. In this approach, the Reggeon in the  $t$ -channel is governed by the Regge trajectory of the  $\rho$  meson, which is well known already [47–52]. We replace the Feynman propagator with the Regge one  $\mathcal{P}_\rho^R$  in the  $t$  channel [47, 51, 52]

$$\frac{1}{t - m_\rho^2} \Rightarrow \mathcal{P}_\rho^R(s, t), \tag{5}$$

where the Regge propagator is defined as

$$\mathcal{P}_\rho^R(s, t) = \left(\frac{s}{s_\rho}\right)^{\alpha_\rho(t)-1} \frac{1}{\sin[\pi\alpha_\rho(t)] \Gamma[\alpha_\rho(t)]}. \quad (6)$$

Here,  $\alpha_\rho(t)$  denotes the Regge trajectory for the  $\rho$  meson.  $s_\rho$  indicates the energy scale parameter for the corresponding Reggeon and is set to be equal to  $1.0 \text{ GeV}^2$ . The Regge trajectory for the  $t$ -channel is taken from Ref. [52]

$$\alpha_\rho(t) = 0.55 + 0.8t. \quad (7)$$

We adopt a degenerate propagator [52, 53] with a constant phase (1). A rotating phase ( $e^{-i\pi\alpha(t)}$ ) is also acceptable. Although the nondegenerate phase ( $(1-\exp[-i\pi\alpha(t)])/2$ ) is general for the  $\rho$  trajectory [54], it is excluded from our consideration because the corresponding result for the  $d\sigma/dt$  reveals a dip structure near  $-t \simeq 0.7 \text{ GeV}^2$  in the range  $E_\gamma = (3.0 - 3.8) \text{ GeV}$  which definitely deviates from the experimental data [31].

In addition, we introduce the scaling factor for the  $\rho$  meson Reggeon exchange

$$C(t) = \frac{a_\rho}{(1 - t/\Lambda_\rho^2)^2}, \quad (8)$$

which are often included to explain experimental values of the cross sections. However, we find that the results are not sensitive to the parameters  $a_\rho$  and  $\Lambda_\rho$  of the scaling factor.

Particle	$J^P$	Mass [GeV]	Width [GeV]	Status
N(1440)	$\frac{1}{2}^+$	1.440	0.300	****
N(1535)	$\frac{1}{2}^-$	1.535	0.150	****
N(1650)	$\frac{1}{2}^-$	1.655	0.150	****
N(1710)	$\frac{1}{2}^+$	1.710	0.100	***

TABLE I. Spin 1/2 resonances [3] for  $\gamma N \rightarrow f_0(500)N$  photoproduction in Model I.

While  $f_0(980)$  photoproduction does not require any contribution from the  $N^*$  resonances because of its high threshold energy, we need to consider them for the explanation of the  $\gamma p \rightarrow f_0(500)p$  reaction. As mentioned earlier, we will take into account the spin 1/2 resonances in Model I:  $N(1440)1/2^+$ ,  $N(1535)1/2^-$ ,  $N(1650)1/2^-$ , and  $N(1710)1/2^+$  as listed in Table I. Since all of them have rather large widths, we will include the finite width in each propagator for the  $N^*$ . Then, the Feynman amplitudes are derived as

$$\begin{aligned} -i\mathcal{M}_{s(N^*(\frac{1}{2}^+))} &= \frac{ef_1gf_0NN^*}{2m_N} \bar{u}(p_2) \frac{i(q_s + m_{N^*})}{s - (m_{N^*} - \frac{i}{2}\Gamma_{N^*})^2} \not{k}_1 \not{\epsilon} u(k_2), \\ -i\mathcal{M}_{s(N^*(\frac{1}{2}^-))} &= \frac{ef_1gf_0NN^*}{2m_N} \bar{u}(p_2) \frac{i(-q_s + m_{N^*})}{s - (m_{N^*} - \frac{i}{2}\Gamma_{N^*})^2} \not{k}_1 \not{\epsilon} u(k_2), \end{aligned} \quad (9)$$

where the first term is the amplitude for the  $N^*$  with positive parity whereas the second one represents that for the negative-parity  $N^*$ . The coupling constants  $f_1$  and  $g_{f_0NN^*}$  denote respectively the generic photocouplings and strong coupling constants for the corresponding  $N^*$  resonances.  $m_{N^*}$  and  $\Gamma_{N^*}$  represent the corresponding masses and the decay widths of the  $N^*$ , respectively. Note that, for the propagators in Eq.(9), we consider the pole positions of the  $N^*$  resonances in the complex plane.

## B. Model II

In Model II, we additionally consider the  $N^*$  resonances with spins 3/2 and 5/2 in the  $s$ -channel. We include the  $N(1520)3/2^-$ ,  $N(1675)5/2^-$ , and  $N(1680)5/2^+$  in the  $s$  channel as listed in Table II [3]. The relevant effective

Particle	$J^P$	Mass [GeV]	Width [GeV]	Status
N(1520)	$\frac{3}{2}^-$	1.525	0.115	****
N(1675)	$\frac{5}{2}^-$	1.675	0.150	****
N(1680)	$\frac{5}{2}^+$	1.685	0.130	****

TABLE II. The excited nucleon resonances [3] for  $f_0(500)$  photoproduction in Model II

Lagrangians for the  $N^*$  resonances are given as follows

$$\begin{aligned}
\mathcal{L}_{\gamma NN^*(\frac{3}{2}^-)} &= \frac{ief_1}{2m_N} \bar{N}_\mu^* F^{\mu\nu} \gamma_\nu N - \frac{ef_2}{(2m_N)^2} \bar{N}_\mu^* F^{\mu\nu} \partial_\nu N + \text{H.c.}, \\
\mathcal{L}_{\gamma NN^*(\frac{5}{2}^\pm)} &= \pm \frac{ef_1}{(2m_N)^2} \bar{N}_{\mu\alpha}^* \partial^\alpha F^{\mu\nu} \Gamma_\nu^{(\mp)} N \pm \frac{ief_2}{(2m_N)^3} \bar{N}_{\mu\alpha}^* \partial^\alpha F^{\mu\nu} \Gamma^{(\mp)} \partial_\nu N + \text{H.c.}, \\
\mathcal{L}_{f_0 NN^*(\frac{3}{2}^-)} &= \frac{gf_0 NN^*}{m_{f_0}} (\partial_\mu f_0) \bar{N} N^{*\mu} + \text{H.c.}, \\
\mathcal{L}_{f_0 NN^*(\frac{5}{2}^\pm)} &= i \frac{gf_0 NN^*}{m_{f_0}^2} \bar{N} (\partial_\mu \partial_\nu f_0) \Gamma^{(\mp)} N^{*\mu\nu} + \text{H.c.}, \tag{10}
\end{aligned}$$

where  $f_1$ ,  $f_2$ , and  $g_{f_0 NN^*}$  denote the photocouplings and the strong coupling constants, respectively. They can be determined by using the experimental data on the photon decay amplitudes and the decay widths  $\Gamma_{N^* \rightarrow f_0(500)N}$ . Then, the Feynman invariant amplitudes for the  $s$ -channel are derived as

$$\begin{aligned}
-i\mathcal{M}_{s(N(1520))} &= ip_1^\mu \bar{u}(p_2) \Delta_{\mu\alpha}(q_s, m_{N^*}) (k_1^\alpha \epsilon^\beta - k_1^\beta \epsilon^\alpha) \\
&\quad \times \left( \frac{ef_1 g_{f_0 NN^*}}{2m_N m_{f_0}} \gamma_\beta + \frac{ef_2 g_{f_0 NN^*}}{4m_N^2 m_{f_0}} k_{2\beta} \right) u(k_2), \\
-i\mathcal{M}_{s(N(1675))} &= \bar{u}(p_2) p_1^\rho p_1^\sigma \gamma_5 \Delta_{\rho\sigma;\mu\alpha}(q_s, m_{N^*}) k_1^\alpha (k_1^\mu \epsilon^\nu - k_1^\nu \epsilon^\mu) \\
&\quad \times \left( \frac{ief_1 g_{f_0 NN^*}}{4m_N^2 m_{f_0}^2} \gamma_\nu + \frac{ief_2 g_{f_0 NN^*}}{8m_N^3 m_{f_0}^2} k_{2\nu} \right) \gamma_5 u(k_2), \\
-i\mathcal{M}_{s(N(1680))} &= -\bar{u}(p_2) p_1^\rho p_1^\sigma \Delta_{\rho\sigma;\mu\alpha}(q_s, m_{N^*}) k_1^\alpha (k_1^\mu \epsilon^\nu - k_1^\nu \epsilon^\mu) \\
&\quad \times \left( \frac{ief_1 g_{f_0 NN^*}}{4m_N^2 m_{f_0}^2} \gamma_\nu + \frac{ief_2 g_{f_0 NN^*}}{8m_N^3 m_{f_0}^2} k_{2\nu} \right) u(k_2), \tag{11}
\end{aligned}$$

where  $\Delta_{\mu\alpha}$  and  $\Delta_{\rho\sigma;\mu\alpha}$  indicate the Rarita-Schwinger propagators for the  $N^*$  resonances with spin 3/2 and 5/2, respectively, defined as [55–58]

$$\begin{aligned}
\Delta_{\mu\alpha}(q, m_{N^*}) &= \frac{i(\not{q} + m_{N^*})}{s - (m_{N^*} - \frac{i}{2}\Gamma_{N^*})^2} S_{\mu\alpha}(q, m_{N^*}), \\
\Delta_{\alpha\beta;\mu\nu}(q, m_{N^*}) &= \frac{i(\not{q} + m_{N^*})}{s - (m_{N^*} - \frac{i}{2}\Gamma_{N^*})^2} S_{\alpha\beta;\mu\nu}(q, m_{N^*}). \tag{12}
\end{aligned}$$

Here,  $S_{\mu\alpha}$ ,  $\bar{g}_{\mu\alpha}$ , and  $\bar{\gamma}_\mu$  are expressed as

$$\begin{aligned}
S_{\mu\alpha}(q, m_{N^*}) &= -\bar{g}_{\mu\alpha} + \frac{1}{3} \bar{\gamma}_\mu \bar{\gamma}_\alpha, \\
S_{\alpha\beta;\mu\nu}(q, m_{N^*}) &= \frac{1}{2} (\bar{g}_{\alpha\mu} \bar{g}_{\beta\nu} + \bar{g}_{\alpha\nu} \bar{g}_{\beta\mu}) - \frac{1}{5} \bar{g}_{\alpha\beta} \bar{g}_{\mu\nu} \\
&\quad - \frac{1}{10} (\bar{\gamma}_\alpha \bar{\gamma}_\mu \bar{g}_{\beta\nu} + \bar{\gamma}_\alpha \bar{\gamma}_\nu \bar{g}_{\beta\mu} + \bar{\gamma}_\beta \bar{\gamma}_\mu \bar{g}_{\alpha\nu} + \bar{\gamma}_\beta \bar{\gamma}_\nu \bar{g}_{\alpha\mu}), \\
\bar{g}_{\mu\alpha} &= g_{\mu\alpha} - \frac{q_\mu q_\alpha}{m_{N^*}^2}, \quad \bar{\gamma}_\mu = \gamma_\mu - \frac{q_\mu \not{q}}{m_{N^*}^2}. \tag{13}
\end{aligned}$$

### C. Parameters and form factors

The coupling constant for the  $\rho NN$  vertex is the most important parameter to describe  $f_0(980)$  photoproduction, since the  $t$ -channel governs the production mechanism of the  $\gamma N \rightarrow f_0(980)N$  reaction. The coupling constant  $g_{\rho NN}$

and  $\kappa_\rho$  are well known from  $NN$  potentials. For example,  $g_{\rho NN} = 3.25$  was used in the full Bonn potential [59], while the Nijmegen group employed  $g_{\rho NN} = 2.76$  [60]. On the other hand, smaller coupling constants  $g_{\rho NN} = 2.6$  and  $\kappa_\rho = 3.7$  have been exploited in Regge models for photoproduction of the pion and of the charged  $\rho^\pm$  meson [63, 64]. We use  $g_{\rho NN} = 3.25$  and the ratio of the vector and tensor couplings  $\kappa_\rho = 6.1$  [59].

The  $f_0(980)NN$  coupling constants is taken from Ref. [65]:  $g_{f_0(980)NN} = 5.8$ . The  $f_0(500)NN$  coupling constant  $g_{f_0(500)NN}$  is a crucial one which explains the mid-range strong attraction in the  $NN$  interaction. Its value is given in a wide numerical range. For example, the full Bonn potential suggests  $g_{\sigma' NN} = 8.46$  [59] with  $m_{\sigma'} = 550$  MeV. The notation  $\sigma'$  in Ref. [59] was introduced to emphasize the fact that  $\sigma'$  represents only an effective description of correlated  $2\pi$  exchange in  $S$  wave. In the one-boson-exchange (OBE) Bonn NN potential, two different  $\sigma$ s were introduced, i.e.  $\sigma_1$  in the isovector ( $T = 1$ ) channel and  $\sigma_2$  in the isoscalar channel ( $T = 0$ ). The charge-dependent OBE Bonn  $NN$  potential has even several different values for different partial waves in  $NN$  scattering [66]. One has to keep in mind that the coupling constant for the  $\sigma NN$  vertex describes effectively whole  $2\pi$  and even  $\pi\rho$  exchanges. On the other hand, the Nijmegen soft-core (NSC) potential includes two different scalar mesons, flavor SU(3) symmetry and ideal mixing being used [67]. Depending on whether the scalar mesons constitute quark-antiquark pairs or tetraquarks, Ref. [67] suggested two different values for the  $\sigma NN$  and  $f_0(980)NN$  coupling constants with different flavor content. Since the  $f_0(500)$  in the present work corresponds to the  $S$ -wave correlated  $2\pi$ , we will take the value of  $g_{\sigma' NN}$  from the full Bonn potential, i.e.  $g_{f_0(500)NN} = 8.46$ . This choice is reasonable, since  $f_0(500)$  in the present work indeed corresponds to the resonance in the  $S$ -wave correlated  $2\pi$  channel. Note that  $\sigma'$ -exchange in the full Bonn potential was later replaced by the explicit  $S$ -wave correlated  $2\pi$ -exchange [61, 62]. Of course, there is one caveat: Since the  $f_0(500)$  meson has a very broad width, a single coupling constant is a rather crude approximation. A more complete work considering  $f_0(500)$  as  $S$ -wave correlated  $2\pi$  resonance will be considered in a future work.

The mass of the  $f_0(500)$  meson brings out another ambiguity in dealing with  $f_0(500)$  photoproduction. Because of the broad width of  $f_0(500)$  ( $\Gamma = (400 - 700)$  MeV), it is rather difficult to determine its mass exactly. The Particle Data Group estimated the pole mass of  $f_0(500)$  to be  $(400 - 500) - i(200 - 350)$  MeV [3]. It implies that we need to examine carefully the  $f_0(500)$  mass dependence of observables. If it is taken to be larger than  $m_{f_0(500)} = 500$  MeV, the threshold energy can be larger than the mass of the  $N(1440)$ . Thus, the total cross section of the  $\gamma N \rightarrow f_0(500)N$  could reveal different behavior from that with the lower value of the  $f_0(500)$  mass. We will discuss in detail the dependence of the total cross section on  $m_{f_0(500)}$  in the next Section.

In order to determine the strong coupling constants for the excited baryons, we assume that the  $f_0(500)$  meson consists mainly of the correlated  $2\pi$  state in  $S$ -wave. Then, we can use the decay modes of  $N^* \rightarrow (\pi^+\pi^-)_{S\text{-wave}}^{I=0}$  to fix the corresponding coupling constants by using the partial decay widths defined as

$$\begin{aligned}\Gamma(N^*(\tfrac{1}{2}^\pm) \rightarrow f_0 N) &= \frac{g_{f_0 NN^*}^2}{4\pi} \frac{|\mathbf{p}|}{m_{N^*}} (E_N \pm m_N), \\ \Gamma(N^*(\tfrac{3}{2}^\pm) \rightarrow f_0 N) &= \frac{1}{3} \frac{g_{f_0 NN^*}^2}{4\pi} \frac{|\mathbf{p}|^3}{m_{N^*} m_{f_0}^2} (E_N \mp m_N), \\ \Gamma(N^*(\tfrac{5}{2}^\pm) \rightarrow f_0 N) &= \frac{2}{15} \frac{g_{f_0 NN^*}^2}{4\pi} \frac{|\mathbf{p}|^5}{m_{N^*} m_{f_0}^4} (E_N \pm m_N),\end{aligned}\tag{14}$$

where the partial decay width,  $\Gamma(N^* \rightarrow f_0 N)$  is given as  $\Gamma_{N^*}^{\text{BW}} \times \text{Br}(N^* \rightarrow f_0 N)$ .  $\Gamma_{N^*}^{\text{BW}}$  denotes the Breit-Wigner total decay width and  $\text{Br}(N^* \rightarrow f_0 N)$  the branching ratio.  $|\mathbf{p}|$  represents the magnitude of the final-state momentum defined as

$$|\mathbf{p}| = \frac{1}{2m_{N^*}} \sqrt{[m_{N^*}^2 - (m_N + m_{f_0})^2][m_{N^*}^2 - (m_N - m_{f_0})^2]}.\tag{15}$$

The results of the strong coupling constants are shown in Table. III

$g_{f_0 NN(1440)}$	$g_{f_0 NN(1535)}$	$g_{f_0 NN(1650)}$	$g_{f_0 NN(1710)}$	$g_{f_0 NN(1520)}$	$g_{f_0 NN(1675)}$	$g_{f_0 NN(1680)}$
$\pm 3.88$	$\pm 2.55$	$\pm 0.96$	$\pm 0.15$	$\pm 0.85$	$\pm 9.85$	$\pm 2.29$

TABLE III. The strong coupling constants for the  $N^*$  resonances. The first four coupling constants correspond to those for the excited nucleons with spin 1/2, whereas the next three ones are those for the  $N^*$  resonances with spin is 3/2 and 5/2.

Concerning the photocoupling constants for  $\rho$ -meson exchange, we use  $g_{\gamma f_0(500)\rho} = 0.25$  [38] from the measurement of the SND Collaboration, and  $g_{\gamma f_0(980)\rho} \approx 0.21$  [68, 69] from the molecular  $K\bar{K}$  model for  $\Gamma_{f_0 \rightarrow \rho\gamma}$  [70]. On the other hand, we can utilize the helicity amplitudes given in the Particle Data Group [3] to find the photocoupling constants

$f_1$  and  $f_2$  for excited nucleons. Since the helicity amplitude are expressed as [71]

$$\begin{aligned}
A_{1/2} \left( \frac{1^\pm}{2} \right) &= \mp \frac{ef_1}{2m_N} \sqrt{\frac{k_\gamma m_{N^*}}{m_N}}, \\
A_{1/2} \left( \frac{3^\pm}{2} \right) &= \mp \frac{e\sqrt{6}}{12} \sqrt{\frac{k_\gamma}{m_N m_{N^*}}} \left[ f_1 + \frac{f_2}{4m_N^2} m_{N^*} (m_{N^*} \mp m_N) \right], \\
A_{3/2} \left( \frac{3^\pm}{2} \right) &= \mp \frac{e\sqrt{2}}{4m_N} \sqrt{\frac{k_\gamma m_{N^*}}{m_N}} \left[ f_1 \mp \frac{f_2}{4m_N} (m_{N^*} \mp m_N) \right], \\
A_{1/2} \left( \frac{5^\pm}{2} \right) &= \pm \frac{e}{4\sqrt{10}} \frac{k_\gamma}{m_N} \sqrt{\frac{k_\gamma}{m_N m_{N^*}}} \left[ f_1 + \frac{f_2}{4m_N^2} m_{N^*} (m_{N^*} \pm m_N) \right], \\
A_{3/2} \left( \frac{5^\pm}{2} \right) &= \pm \frac{e}{4\sqrt{5}} \frac{k_\gamma}{m_N^2} \sqrt{\frac{k_\gamma m_{N^*}}{m_N}} \left[ f_1 \pm \frac{f_2}{4m_N} (m_{N^*} \pm m_N) \right],
\end{aligned} \tag{16}$$

where  $k_\gamma$  stands for the photon decay momentum in the center of mass (CM) frame and is expressed as

$$k_\gamma = \frac{m_{N^*}^2 - m_N^2}{2m_{N^*}}, \tag{17}$$

we obtain the photocouplings for the electromagnetic transitions  $N^* \rightarrow \gamma N$  as listed in Table IV.

$f_{\gamma NN(1440)}$	$f_{\gamma NN(1535)}$	$f_{\gamma NN(1650)}$	$f_{\gamma NN(1710)}$
0.47	0.81	0.28	-0.24
$f_{1\gamma NN(1520)}$	$f_{2\gamma NN(1520)}$		
4.63	-4.92		
$f_{1\gamma NN(1675)}$	$f_{2\gamma NN(1675)}$	$f_{1\gamma NN(1680)}$	$f_{2\gamma NN(1680)}$
-1.34	-2.28	15.24	-13.47

TABLE IV. The photon coupling constants for the  $N^*$  resonances whose spin is 1/2 are listed in the first row. In the second and the third row the photon coupling constants for the  $N^*$  resonances whose spin is 3/2 and 5/2, respectively, are listed.

A hadron has a spatial size, which can be characterized by the phenomenological form factors. Hence, one has to introduce them at each baryon-baryon-meson vertex. Note that each amplitude of  $N$  exchanges does not satisfy the gauge invariance in the  $s$ - and  $u$ -channels, but the sum does. To restore the gauge invariance, we modify the Born scattering amplitudes as

$$\mathcal{M}_{\text{Born}} = \mathcal{M}_t^{\text{Regge}} + (\mathcal{M}_s + \mathcal{M}_u)F_c^2(s, u), \tag{18}$$

where a common form factor is introduced as [72]

$$F_c(s, u) = F(s) + F(u) - F(s)F(u), \tag{19}$$

with

$$F(q^2) = \frac{\Lambda^4}{\Lambda^4 + (q^2 - m_{ex}^2)^2}. \tag{20}$$

Here,  $q$  indicates the off-shell four-momentum for an exchanged hadron,  $m_{ex}$  stands for its mass, and  $\Lambda$  denotes a cutoff parameter. As for the form factors in  $N^*$  exchange, we also use Eq. (20). However, it is not sufficient to preserve the unitarity for the  $N^*$  resonances with spin 3/2 and 5/2, since the corresponding amplitudes show much stronger  $q^2$  dependence so that they are divergent as  $E_\gamma$  increases. Thus, in order to tame the divergence, we will employ a Gaussian type of the form factor for both  $N(1520)3/2^-$ ,  $N(1675)5/2^-$  and  $N(1680)5/2^+$ -exchange in the  $s$ -channel, defined as

$$F(q^2) = \exp \left[ -\frac{(q^2 - m_{N^*}^2)^2}{\Lambda^4} \right]. \tag{21}$$



### III. RESULTS AND DISCUSSION

We are now in a position to present the numerical results of our work. Since there exists the experimental data on the differential cross section of the  $\gamma N \rightarrow f_0(980)N$  reaction [31], we start with  $f_0(980)$  photoproduction.

#### A. $\gamma N \rightarrow f_0(980)N$

In order to describe the experimental data on  $d\sigma/dt$  of the  $\gamma N \rightarrow f_0(980)N$  process [31], we fix the scaling factor in Eq. (8) to be  $a_\rho = 9.0$ . As is well known, while the Regge approach describes the energy dependence very well, it cannot determine the absolute magnitude of the cross sections. Thus, it is inevitable to introduce the scale parameter  $a_\rho$  to fit the cross sections. The value of the cutoff parameter  $\Lambda_\rho$  is selected to be 1 GeV that is a typical order of the cut-off value. We do not fit it to avoid additional ambiguity. The cutoff parameters in  $N$ - and  $N^*$ -exchanges are chosen as  $\Lambda_N = 0.8$  GeV and  $\Lambda_{N^*} = 1.0$  GeV. The values of  $\Lambda_{\rho, N^*}$  are also typical ones. Note that the cutoff value for the backward scattering amplitude is usually smaller than that for the forward scattering one in the literature [44, 45]. Furthermore, the experimental data for the backward region are currently not available. So, we simply choose these values without any fitting procedure.

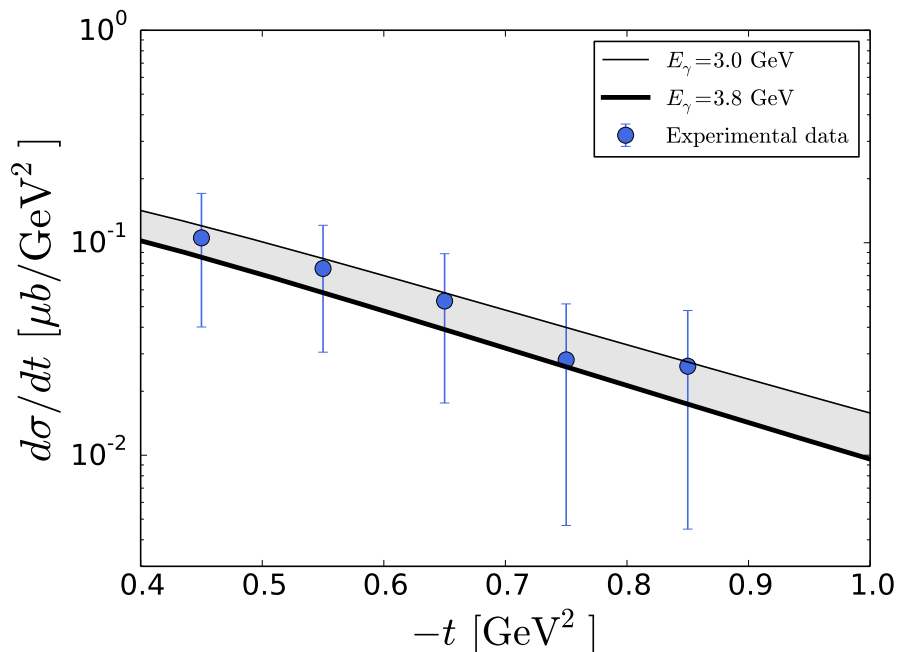


FIG. 2. Differential cross section of the  $\gamma N \rightarrow f_0(980)N$  reaction as a function  $t$  in the range of  $E_\gamma = (3.0 - 3.8)$  GeV. The shaded band represents the present result. The experimental data are taken from Ref. [31].

Figure 2 draws the differential cross section  $d\sigma/dt$  of the  $\gamma N \rightarrow f_0(980)N$  reaction. The experimental data are taken from Ref. [31], where  $d\sigma/dt$  were measured within the range of the photon energy  $E_\gamma = (3.0 - 3.8)$  GeV. In order to compare the present results with the data, we present the results as the shaded band of which the width represents the corresponding region of  $E_\gamma$ . Considering the large experimental uncertainty, the results describe the data very well. Note that the  $t$ -dependence is governed by  $\rho$ -Reggeon exchange in the  $t$  channel.

In Fig. 3, we depict the contribution of each channel to the total cross section of the  $\gamma N \rightarrow f_0(980)N$  reaction. The  $\rho$ -Reggeon exchange dominates over the  $s$ - and  $u$ -channel diagrams, whereas the  $N$  exchanges have small effects in the whole energy region.

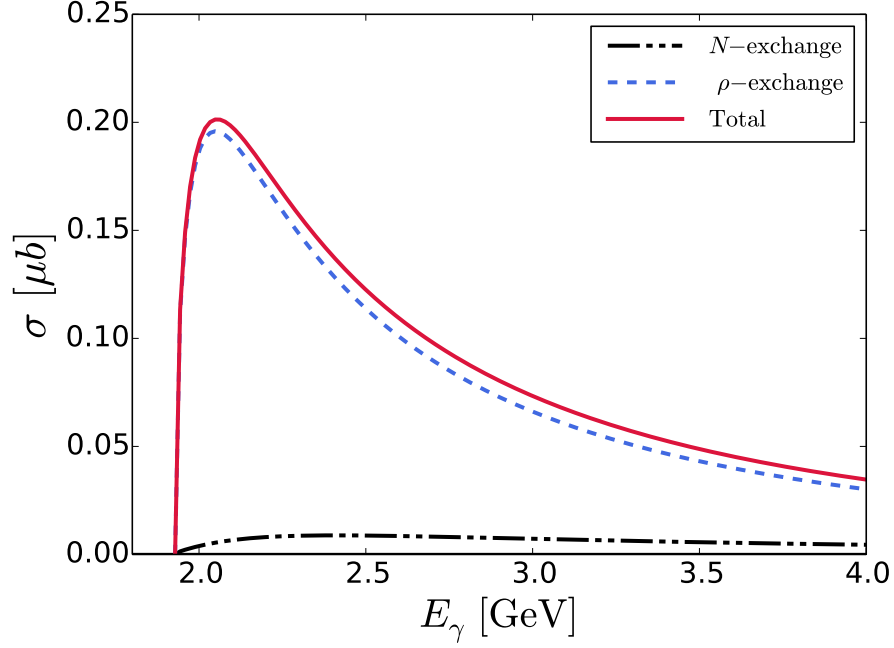


FIG. 3. Total cross section of the  $\gamma N \rightarrow f_0(980)N$  reaction. The dashed curve depicts the contribution of  $\rho$ -Reggeon exchange in the  $t$  channel, whereas the dot-dashed and double-dot-dashed ones draw those of  $N$ -Reggeon exchange and of  $N$  exchange in the  $u$  and  $s$  channels, respectively. The solid curve represents the total contribution.

### B. $\gamma N \rightarrow f_0(500)N$

The parameters for  $f_0(500)$  photoproduction in the  $t$ ,  $s$ , and  $u$  channels are kept to be the same as those in the case of the  $\gamma N \rightarrow f_0(980)N$  reaction. However, the  $N^*$  resonances play essential roles in describing the  $\gamma N \rightarrow f_0(500)N$  reaction in particular in the vicinity of threshold.

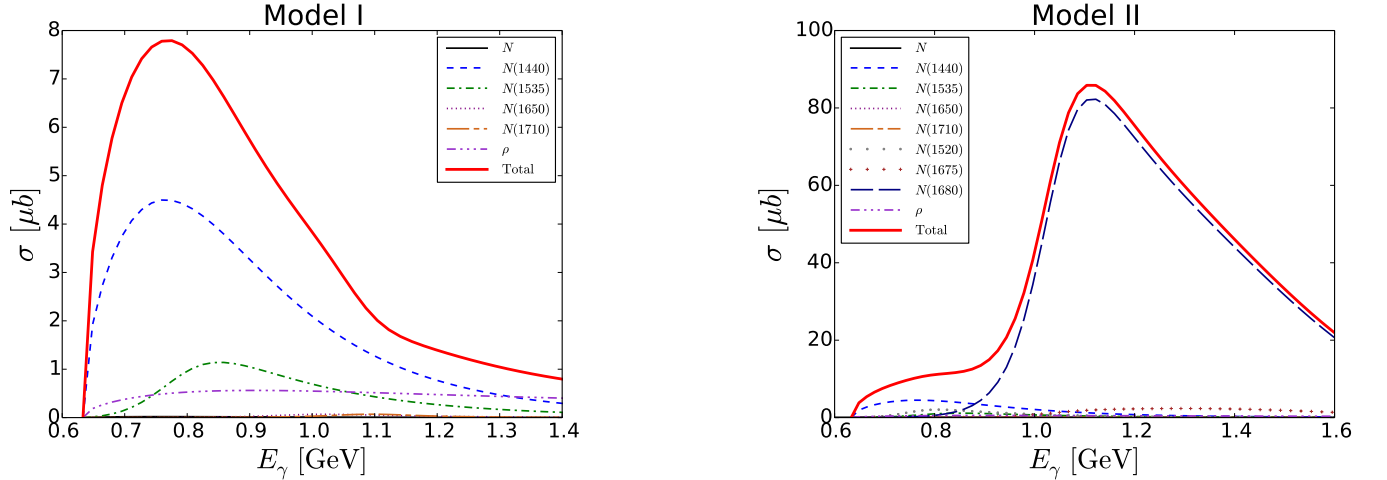


FIG. 4. Total cross sections for the  $\gamma N \rightarrow f_0(500)N$  reaction as a function of  $E_\gamma$ . In the left panel, the results from Model I are drawn, whereas in the right panel those from Model II are depicted. Each contribution is distinguished by different types of the curves.

We need to delve into the physical reasons for Model I. The  $N(1440)1/2^+$  and  $N(1535)1/2^-$  resonances increase

the total cross section of the  $\gamma N \rightarrow f_0(500)N$  reaction near threshold. As shown in the left panel of Fig. 4, the most dominant contribution arises from the  $N(1440)1/2^+$  resonance. Since the  $N(1650)1/2^-$  and  $N(1710)1/2^+$  resonances have relatively smaller strong coupling constants as well as photocouplings as listed in Tables III and IV, the effect of these resonances is tiny. Interestingly, the contribution of the  $\rho$  Reggeon in the  $t$  channel is rather suppressed. The effect of  $N$  exchanges in the  $s$  and  $u$  channels is much smaller than that of  $\rho$ -Reggeon exchange through the whole energy region. The magnitude of the total cross section for  $f_0(500)$  photoproduction is about 40 times larger than that for  $f_0(980)$  production in the case of Model I.

The right panel of Fig. 4 depicts the results of the total cross section for the  $\gamma N \rightarrow f_0(500)N$  reaction from Model II, where the  $N^*$  resonances with higher spins are added in the  $s$  channel in addition. The  $N(1680)5/2^+$  resonance in the  $s$  channel yields a remarkably large contribution to the total cross section of  $f_0(500)$  photoproduction, so that its magnitude reaches even about  $80 \mu\text{b}$  around  $E_\gamma \approx 1.1$  GeV. There is at least one clear reason for this large contribution of the  $N(1680)5/2^+$ . Firstly, the photocouplings of the  $N(1680)5/2^+$  are very large, as shown in Table IV, which come from the large values of the experimental data on the photon decay amplitudes  $A_{1/2}$  and  $A_{3/2}$  [3]. The value of  $f_{1\gamma NN(1680)}$  is even about 32 times larger than that of  $f_{1\gamma NN(1440)}$ . Moreover, the size of the strong coupling constant for the  $f_0(500)NN(1680)$  vertex is comparable to that of  $g_{f_0(500)NN(1440)}$ . Note that even though the value of  $g_{f_0(500)NN(1675)}$  is rather large, the  $N(1675)5/2^-$  resonance has almost no effect on the total cross section because of its negative parity. The results are not so sensitive to variations of the cut-off masses. In this regard, the contribution of the  $N(1680)5/2^+$  resonance discussed here seems to be robust. Thus, it would be indeed of great interest if one could justify experimentally whether the  $N(1680)5/2^+$  resonance plays such a dominant role in describing the  $\gamma N \rightarrow f_0(500)N$  reaction.

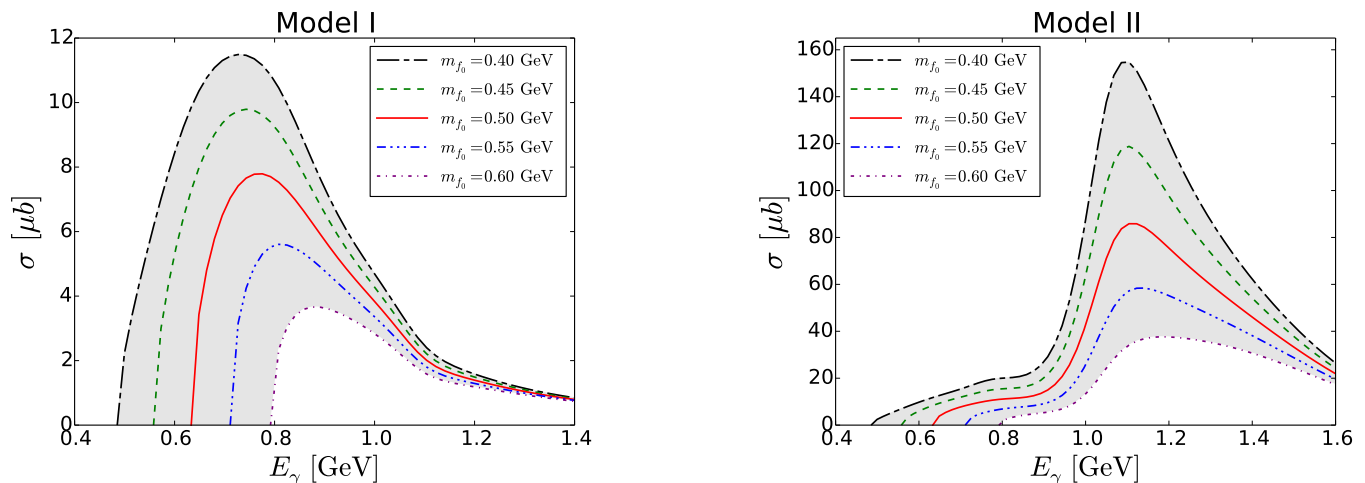


FIG. 5.  $f_0(500)$  mass dependence of the total cross section for the  $\gamma N \rightarrow f_0(500)N$  reaction both in Model I and Model II.

As mentioned briefly in Introduction, the uncertainty in the mass of  $f_0(500)$  is so large on account of its broad width, it is quite unclear to settle the threshold energy. The PDG data has it that the pole mass of  $f_0(500)$  is  $[(400 - 550) - i(200 - 350)]$  MeV [3]. In fact, the estimated mass of  $f_0(500)$  is given in a wide range of its values, as listed in Ref. [3]. Thus, we have to examine the dependence of the total cross section on the mass of  $f_0(500)$ . In the left panel of Fig. 5, we draw the results of the total cross section of the  $\gamma N \rightarrow f_0(500)N$  reaction from Model I with various values of  $m_{f_0}$  given between 0.4 GeV and 0.6 GeV. As expected, the smaller values of  $m_{f_0}$  produce the larger magnitudes of the total cross section. Note that if one uses the value of  $m_{f_0}$  larger than 500 MeV, the  $N(1440)1/2^+$  will be excluded because of the larger threshold energy. Thus, the total cross section starts to get reduced when the value of  $m_{f_0}$  is larger than 500 MeV. In the present work, we will take  $m_{f_0(500)} = 500$  MeV from now on.

In Figs. 4 and 5, we mainly have examined the total cross section of  $f_0(500)$  photoproduction in the vicinity of the threshold energy. We now delve into the dependence of the total cross section on  $E_\gamma$  from the threshold energy through 10 GeV in the log scale. In the left panel of Fig. 6, we show the behavior of each contribution from Model I as  $E_\gamma$  increases. As expected, all the resonance effects are diminished quickly with the photon energy increased, while the  $\rho$ -Reggeon in the  $t$  channel takes over the contributions of all the  $N^*$  resonances around  $E_\gamma \approx 2$  GeV and then dictates the dependence of the total cross section on  $E_\gamma$ . The  $t$ -channel Reggeon ensures the unitarity of the total cross section, as shown in Fig. 6. In the limit of  $s \rightarrow \infty$ , the unpolarized sum of the Regge amplitude complies with

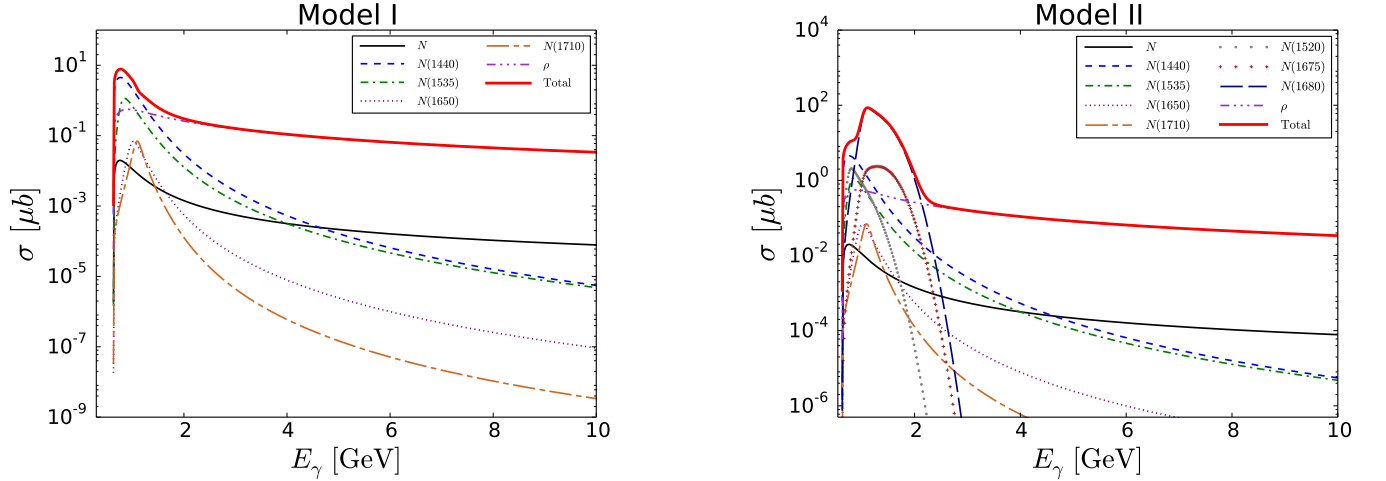


FIG. 6. Total cross sections for the  $\gamma N \rightarrow f_0(500)N$  reaction as a function of  $E_\gamma$  in the log scale. In the left panel, the results from Model I are drawn, whereas in the right panel those from Model II are depicted. Each contribution is distinguished by different types of the curves.

the following asymptotic behavior

$$\lim_{s \rightarrow \infty} \sum_{\text{pol}} |\mathcal{M}_t^{\text{Regge}}(s, t)|^2 \propto s^{2\alpha_\rho(t)}. \quad (22)$$

Thus, if one further increases  $E_\gamma$ , the contribution of the  $\rho$  meson starts to decrease, satisfying the asymptotic behavior of Eq. (22). The right panel of Fig. 6 shows the results from Model II. Similarly, the contributions of most  $N^*$  resonances fall off very fast as  $E_\gamma$  increases. The effect of the  $N(1680)5/2^+$  lessens continuously after  $E_\gamma \approx 1.2$  GeV, and then becomes smaller than those of the  $\rho$  Reggeons around  $E_\gamma \approx 2$  GeV. Thus, the  $N^*$  resonances come into play only near the threshold region as anticipated.

In the upper panel of Fig. 7, the results of the differential cross section  $d\sigma/d\cos\theta$  from Model I are plotted as functions of  $\cos\theta$ , as the photon energy  $E_\gamma$  is varied from 0.8 GeV through 3.5 GeV. Usually, the  $s$ -channel contributions including all  $N^*$  resonances with spin 1/2 do not show any  $\cos\theta$  dependence. Note that Model I does not contain any  $N^*$  resonances with higher spins. Nevertheless, the results of  $d\sigma/d\cos\theta$  exhibit different peculiarities. The differential cross section  $d\sigma/d\cos\theta$  in the forward region grows as  $E_\gamma$  increases. However, the value of  $d\sigma/d\cos\theta$  almost vanishes at the very forward angle at higher values of  $E_\gamma$ . This arises from the structure of the amplitude of  $\rho$  exchange in Eq. (3). Model II yields rather different results from those based on Model I. Since the  $N(1680)5/2^+$  resonance is the most dominant one from the threshold energy through 1.5 GeV as shown in Fig. 4, and it has spin 5/2 with positive parity, we expect that it will have a certain effect on the  $\cos\theta$  dependence of the differential cross section. Indeed, it steers  $d\sigma/d\cos\theta$  up to  $E_\gamma \approx 2.1$  GeV, as shown in the lower panel of Fig. 7. As  $E_\gamma$  increases more than 1.7 GeV, the  $\rho$  Reggeon gains control of the  $\cos\theta$  dependence of the differential cross section, so that we have more or less the same results as in the upper panel of Fig. 7.

Figure 8 draws the results of the differential cross section  $d\sigma/dt$  as a function of  $-t$  in the range of  $E_\gamma = (3.0 - 3.8)$  GeV, so that we can directly compare them with those of  $f_0(980)$  photoproduction. The  $t$  dependence is almost the same as that of the  $f_0(980)$  case, because we have exactly the same  $\rho$ -Reggeon and  $N$  exchanges. The only differences come from the coupling constants. The contributions of the  $N^*$  resonances are all suppressed in this region of the photon energies. The magnitude of  $d\sigma/dt$  is approximately 2 times larger than that of  $f_0(980)$  photoproduction on account of different coupling constants. Note that the differential cross section  $d\sigma/dt$  obeys the following asymptotic behavior

$$\lim_{s \rightarrow \infty} \frac{d\sigma}{dt}(t \rightarrow 0) \propto s^{2\alpha_\rho(0)-2} \quad (23)$$

and the result shown in Fig. 8 satisfies Eq. (23).

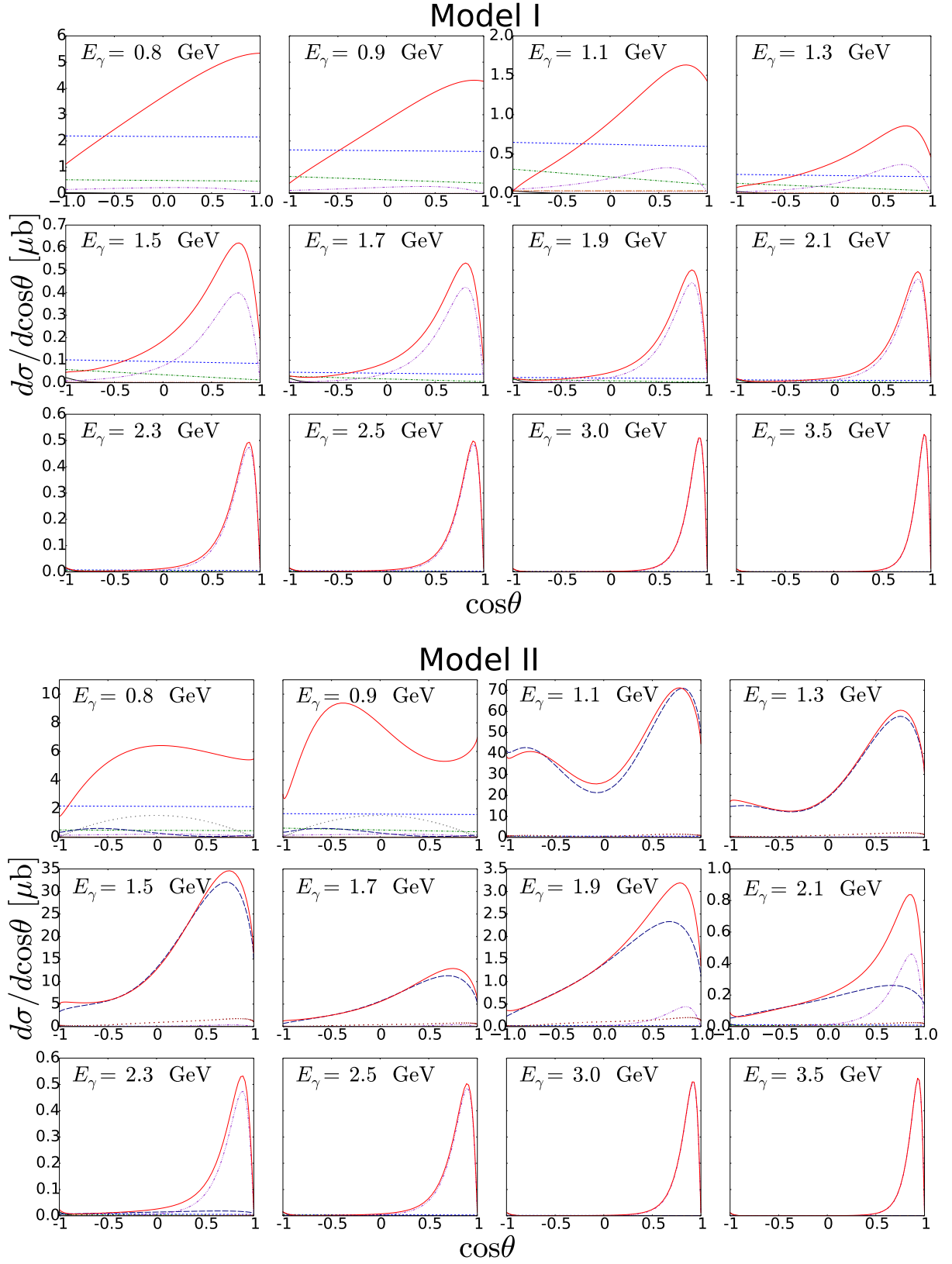


FIG. 7. Differential cross section for the  $\gamma N \rightarrow f_0(500)N$  reaction as a function  $\cos\theta$  with the photon energy  $E_\gamma$  changed from 0.8 GeV to 3.5 GeV. The results from Model I are drawn in the upper panel, whereas those from Model II are depicted in the lower panel. Notations are the same as in Fig. 4.

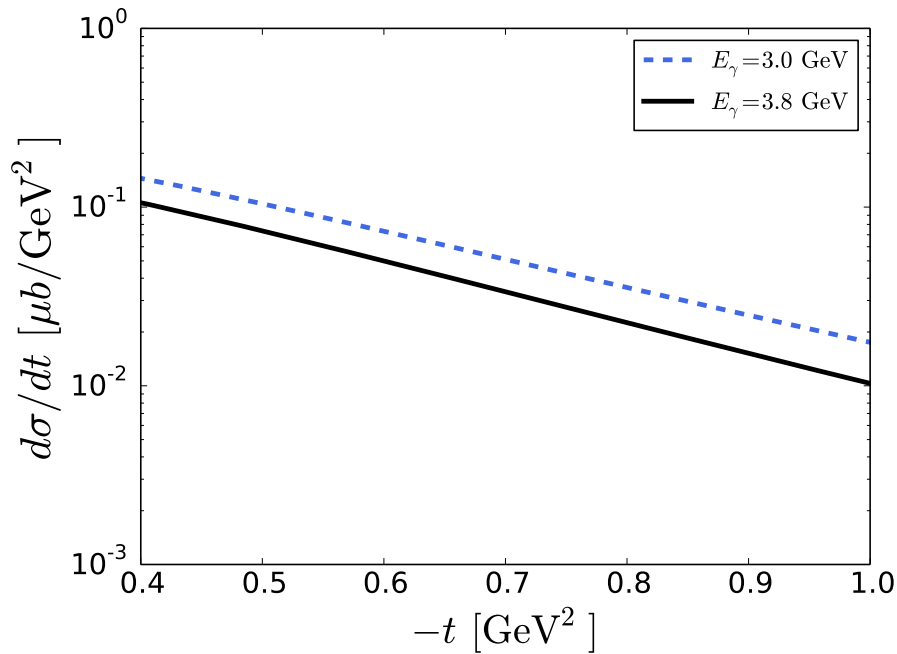


FIG. 8. Differential cross section for the  $\gamma N \rightarrow f_0(500)N$  reaction as a function  $t$  at two different photon energies, i.e.  $E_\gamma = 3.0$  GeV and  $E_\gamma = 3.8$  GeV. The solid curve represents the result at  $E_\gamma = 3.8$  GeV, whereas the dashed one plots that at  $E_\gamma = 3.0$  GeV.

#### IV. SUMMARY AND CONCLUSION

We aimed in this work at investigating  $f_0(500)$  and  $f_0(980)$  photoproduction, based on a hybridized Regge model. We first described the differential cross section  $d\sigma/dt$  for the  $\gamma N \rightarrow f_0(980)N$  reaction, compared with the recent experimental data on it. We fixed the relevant Regge parameters by reproducing the data. We introduced the  $N^*$  contribution in the  $s$  channel to study the production mechanism of the  $\gamma N \rightarrow f_0(500)N$  reaction. Since its threshold energy is much smaller than  $f_0(980)$  photoproduction, there exist several  $N^*$  resonances that can decay into  $(\pi\pi)_{S\text{-wave}}^{I=0}N$ . Assuming that  $f_0(500)$  is much stronger than the background of the  $(\pi\pi)_{S\text{-wave}}^{I=0}$  channel, we were able to find the strong coupling constants for the  $f_0(500)NN^*$  vertices. The photocouplings of the  $N^*$  resonances were determined by using the experimental data on the corresponding photon decay amplitudes. The cut-off masses for the form factors were fixed to be 1.0 GeV to avoid additional ambiguity. In dealing with these  $N^*$  resonances, we constructed Model I and Model II. Model I included those with spin 1/2 only, while Model II was built in such a way that more  $N^*$  resonances with higher spins were added to Model I. Near threshold, we found that the  $N(1440)1/2^+$  and  $N(1535)1/2^-$  were dominant ones in Model I, whereas the effects of other  $N^*$  resonances were almost negligible. In Model II, the contribution of the  $N(1680)5/2^+$  dictates the total cross section of the  $\gamma N \rightarrow f_0(500)N$  reaction. Remarkably, the  $N(1680)5/2^+$  resonance enhances the magnitude of the total cross section up to about  $80 \mu\text{b}$ . The main reason comes from the large value of its photon couplings. The strong coupling constant of the  $N(1680)5/2^+$  is also relatively large. Since the mass of the  $f_0(500)$  meson is not precisely fixed because of its large width, we examined the dependence of the total cross section on its mass in the range of (400 – 600) MeV. As expected, small the  $f_0(500)$  mass was, the larger the total cross section was in Model I and Model II. If  $E_\gamma$  increases, then the  $N^*$  contribution fade away very fast, so that  $\rho$ -Reggeon exchange takes over the control as in the case of  $f_0(980)$  photoproduction. We also computed the differential cross section  $d\sigma/d\cos\theta$ . While the contributions of the  $N^*$  resonances in the  $s$  channel are rather flat in the case of Model I,  $N(1680)5/2^+$  governs  $\cos\theta$  dependence again because of its high spin. Finally, we computed the differential cross section  $d\sigma/dt$  for the  $\gamma N \rightarrow f_0(500)N$  reaction. The results showed that the  $t$  dependence and the magnitude looked very similar to those for  $f_0(980)$  photoproduction.

Though it is very difficult to study  $f_0(500)$  photoproduction experimentally, it is still of great importance to study the production mechanism of the  $\gamma N \rightarrow f_0(500)N$  reaction, since it cast light on the structure of the  $N^*$  resonances as investigated in the present work. It also provides a certain clue in studying more complicated processes with three-particle final states such as  $\gamma N \rightarrow (\pi\pi)_{S\text{-wave}}^{I=0}N$  in the future.

## ACKNOWLEDGMENTS

H-Ch.K. is grateful to M. V. Polyakov and the members of TPII in Ruhr-Universität Bochum for valuable discussions and hospitality during his visit, where part of the work has been carried out. The present work was supported by Basic Science Research Program through the National Research Foundation of Korea funded by the Ministry of Education, Science and Technology (Grant Number: NRF-2015R1D1A1A01060707). S.H.K acknowledges support from the Young Scientist Training Program at the Asia Pacific Center for Theoretical Physics by the Korea Ministry of Education, Science, and Technology, Gyeongsangbuk-Do and Pohang City.

- 
- [1] C. Amsler and N. A. Tornqvist, Phys. Rept. **389**, 61 (2004).  
 [2] D. V. Bugg, Phys. Rept. **397**, 257 (2004).  
 [3] C. Patrignani et al. (Particle Data Group), Chin. Phys. C **40**, 100001 (2016).  
 [4] J. R. Pelaez, Phys. Rept. **658**, 1 (2016).  
 [5] P. Minkowski and W. Ochs, Eur. Phys. J. C **9**, 283 (1999).  
 [6] W. Ochs, J. Phys. G **40**, 043001 (2013).  
 [7] G. Mennessier, S. Narison and X. G. Wang, Phys. Lett. B **688** (2010) 59.  
 [8] R. L. Jaffe, Phys. Rev. D **15**, 267 (1977).  
 [9] L. Maiani, F. Piccinini, A. D. Polosa and V. Riquer, Phys. Rev. Lett. **93**, 212002 (2004).  
 [10] G. 't Hooft, G. Isidori, L. Maiani, A. D. Polosa and V. Riquer, Phys. Lett. B **662**, 424 (2008).  
 [11] G. Eichmann, C. S. Fischer and W. Heupel, Phys. Lett. B **753**, 282 (2016).  
 [12] D. Lohse, J. W. Durso, K. Holinde and J. Speth, Nucl. Phys. A **516**, 513 (1990).  
 [13] J. A. Oller, E. Oset and J. R. Pelaez, Phys. Rev. D **59**, 074001 (1999) Erratum: [Phys. Rev. D **60**, 099906 (1999)] Erratum: [Phys. Rev. D **75**, 099903 (2007)] 10.1103/PhysRevD.75.099903 [hep-ph/9804209].  
 [14] H. X. Chen, A. Hosaka and S. L. Zhu, Phys. Rev. D **76**, 094025 (2007).  
 [15] D. Black, A. H. Fariborz, F. Sannino and J. Schechter, Phys. Rev. D **59**, 074026 (1999).  
 [16] T. Kunihiro *et al.* [SCALAR Collaboration], Phys. Rev. D **70**, 034504 (2004).  
 [17] M. Wakayama, T. Kunihiro, S. Muroya, A. Nakamura, C. Nonaka, M. Sekiguchi and H. Wada, Phys. Rev. D **91**, no. 9, 094508 (2015).  
 [18] J. Soto, P. Talavera and J. Tarrus, Nucl. Phys. B **866**, 270 (2013).  
 [19] B. Hyams *et al.*, Nucl. Phys. B **64**, 134 (1973).  
 [20] S. D. Protopopescu *et al.*, Phys. Rev. D **7**, 1279 (1973).  
 [21] G. Grayer *et al.*, Nucl. Phys. B **75**, 189 (1974).  
 [22] L. Rosselet *et al.*, Phys. Rev. D **15** (1977) 574.  
 [23] J. R. Batley *et al.* [NA48-2 Collaboration], Eur. Phys. J. C **70** (2010) 635.  
 [24] E. M. Aitala *et al.* [E791 Collaboration], Phys. Rev. Lett. **86**, 770 (2001).  
 [25] G. Bonvicini *et al.* [CLEO Collaboration], Phys. Rev. D **76**, 012001 (2007).  
 [26] M. Ablikim *et al.* [BES Collaboration], Phys. Lett. B **598**, 149 (2004).  
 [27] M. Ablikim *et al.* [BES Collaboration], Phys. Lett. B **645**, 19 (2007).  
 [28] M. Hoferichter, D. R. Phillips and C. Schat, Eur. Phys. J. C **71**, 1743 (2011).  
 [29] D. Barberis *et al.* [WA102 Collaboration], Phys. Lett. B **462**, 462 (1999).  
 [30] M. V. Polyakov and V. V. Vereshagin, Eur. Phys. J. A **12**, 349 (2001).  
 [31] M. Battaglieri *et al.* [CLAS Collaboration], Phys. Rev. Lett. **102**, 102001 (2009).  
 [32] M. Battaglieri *et al.* [CLAS Collaboration], Phys. Rev. D **80**, 072005 (2009).  
 [33] JLab Experiment CLAS Database, <http://clasweb.jlab.org/physicsdb/intro.html>  
 [34] C. R. Ji, R. Kaminski, L. Lesniak, A. Szczepaniak and R. Williams, Phys. Rev. C **58**, 1205 (1998).  
 [35] A. Donnachie and Y. S. Kalashnikova, arXiv:1507.07408 [hep-ph].  
 [36] S. I. Dolinsky *et al.*, Phys. Rept. **202**, 99 (1991).  
 [37] I. B. Vasserman *et al.*, Sov. J. Nucl. Phys. **47**, 1035 (1988) [Yad. Fiz. **47**, 1635 (1988)].  
 [38] M. N. Achasov *et al.*, (SND Collaboration), Phys. Lett. B **537**, 201 (2002).  
 [39] R. R. Akhmetshin *et al.* [CMD-2 Collaboration], Phys. Lett. B **648**, 28 (2007).  
 [40] S. H. Kim, A. Hosaka, H.-Ch. Kim, H. Noumi, and K. Shirotori, PTEP **2014**, 103D01 (2014).  
 [41] S. H. Kim, A. Hosaka, H.-Ch. Kim and H. Noumi, Phys. Rev. D **92**, 094021 (2015).  
 [42] S. H. Kim, H.-Ch. Kim, and A. Hosaka, Phys. Lett. B **763**, 358 (2016).  
 [43] H. Y. Ryu, A. I. Titov, A. Hosaka, and H.-Ch. Kim, PTEP **2014**, 023D03 (2014).  
 [44] S. H. Kim, S. i. Nam, Y. Oh, and H.-Ch. Kim, Phys. Rev. D **84**, 114023 (2011).  
 [45] S. H. Kim, S. i. Nam, A. Hosaka, and H.-Ch. Kim, Phys. Rev. D **88**, 054012 (2013).  
 [46] K. Nakayama, Y. Oh, and H. Habermann, Phys. Rev. C **74**, 035205 (2006).  
 [47] A. Donnachie, H. G. Dosch, P. V. Landshoff and O. Nachtmann, *Pomeron Physics and QCD* (Cambridge University Press, New York, 2002).

- [48] C. Schmid, Phys. Rev. Lett. **20**, 689 (1968).
- [49] J. A. Shapiro, Phys. Rev. **179**, 1345 (1969).
- [50] J. D. Jackson, Rev. Mod. Phys. **42**, 12 (1970).
- [51] L. Sertorio and L. L. Wang, Phys. Rev. **178**, 2462 (1969).
- [52] M. Guidal, J. M. Laget and M. Vanderhaeghen, Nucl. Phys. A **627**, 645 (1997).
- [53] J. M. Laget, Phys. Rev. C **72**, 022202 (2005).
- [54] P D B Collins, A D Martin, and R H Dalitz, Hadron interactions (Bristol, Adam Hilger, 1984).
- [55] R. E. Behrends and C. Fronsdal, Phys. Rev. **106**, 345 (1957).
- [56] J. G. Rushbrooke, Phys. Rev. **143**, 1345 (1966).
- [57] S. J. Chang, Phys. Rev. **161**, 1308 (1967).
- [58] Y. Oh, J. Korean Phys. Soc. **59**, 3344 (2011).
- [59] R. Machleidt, K. Holinde and C. Elster, Phys. Rept. **149**, 1 (1987).
- [60] T. A. Rijken, Phys. Rev. C **73**, 044007 (2006).
- [61] H.-Ch. Kim, J. W. Durso and K. Holinde, Phys. Rev. C **49**, 2355 (1994).
- [62] A. Reuber, K. Holinde, H.-Ch. Kim and J. Speth, Nucl. Phys. A **608**, 243 (1996).
- [63] B. G. Yu, T. K. Choi and W. Kim, Phys. Rev. C **83**, 025208 (2011).
- [64] B. G. Yu and K. J. Kong, arXiv:1604.03691 [nucl-th].
- [65] M. Schumacher, Eur. Phys. J. A **34**, 293 (2007)
- [66] R. Machleidt, Phys. Rev. C **63**, 024001 (2001).
- [67] T. A. Rijken, V. G. J. Stoks and Y. Yamamoto, Phys. Rev. C **59**, 21 (1999).
- [68] Y. Kalashnikova, A. E. Kudryavtsev, A. V. Nefediev, J. Haidenbauer, and C. Hanhart, Phys. Rev. C **73**, 045203 (2006).
- [69] T. Branz, T. Gutsche, and V. E. Lyubovitskij, Eur. Phys. J. A **37**, 303 (2008).
- [70] I. T. Obukhovskiy, A. Faessler, D. K. Fedorov, T. Gutsche, V. E. Lyubovitskij, V. G. Neudatchin, and L. L. Sviridova, Phys. Rev. D **81**, 013007 (2010).
- [71] Y. Oh, C. M. Ko and, K. Nakayama, Phys. Rev. C **77**, 045204 (2008).
- [72] R. M. Davidson and R. Workman, Phys. Rev. C **63**, 025210 (2001).